Diffusion-Weighted MRI of the Liver in Patients With Chronic Liver Disease: A Comparative Study Between Different Fitting Approaches and Diffusion Models

Jiqing Huang, MS,[1] Benjamin Leporq, PhD,[1] Valérie Hervieu, MD,[2] Jérôme Dumortier, MD, PhD,[3] Olivier Beuf, PhD,[1*] and Hélène Ratiney, PhD[1]

Background: Diffusion-weighted imaging (DWI) has been considered for chronic liver disease (CLD) characterization. Grading of liver fibrosis is important for disease management.
Purpose: To investigate the relationship between DWI's parameters and CLD-related features (particularly regarding fibrosis assessment).
Study Type: Retrospective.
Subjects: Eighty-five patients with CLD (age: 47.9 ± 15.5, 42.4% females).
Field Strength/Sequence: 3-T, spin echo-echo planar imaging (SE-EPI) with 12 *b*-values (0–800 s/mm^2).
Assessment: Several models statistical models, stretched exponential model, and intravoxel incoherent motion were simulated. The corresponding parameters (D_s, σ, DDC, α, f, D, D^*) were estimated on simulation and in vivo data using the nonlinear least squares (NLS), segmented NLS, and Bayesian methods. The fitting accuracy was analyzed on simulated Rician noised DWI. In vivo, the parameters were averaged from five central slices entire liver to compare correlations with histological features (inflammation, fibrosis, and steatosis). Then, the differences between mild (F0–F2) or severe (F3–F6) groups were compared respecting to statistics and classification. A total of 75.3% of patients used to build various classifiers (stratified split strategy and 10-folders cross-validation) and the remaining for testing.
Statistical Tests: Mean squared error, mean average percentage error, spearman correlation, Mann–Whitney *U*-test, receiver operating characteristic (ROC) curve, area under ROC curve (AUC), sensitivity, specificity, accuracy, precision. A *P*-value <0.05 was considered statistically significant.
Results: In simulation, the Bayesian method provided the most accurate parameters. In vivo, the highest negative significant correlation (D_s, steatosis: $r = -0.46$, D^*, fibrosis: $r = -0.24$) and significant differences (D_s, σ, D^*, f) were observed for Bayesian fitted parameters. Fibrosis classification was performed with an AUC of 0.92 (0.91 sensitivity and 0.70 specificity) with the aforementioned diffusion parameters based on the decision tree method.
Data Conclusion: These results indicate that Bayesian fitted parameters may provide a noninvasive evaluation of fibrosis with decision tree.
Evidence Level: 1
Technical Efficacy: Stage 1

J. MAGN. RESON. IMAGING 2024;59:894–906.

Chronic liver disease (CLD) represents a broad spectrum of diseases involving different etiologies (eg, nonalcoholic steatosis, viral hepatitis, and hemochromatosis). These diseases are characterized by histological features such as inflammation, fibrosis, steatosis, ballooning, or iron overload. Among them, liver fibrosis is a key feature since it affects the prognosis and

View this article online at wileyonlinelibrary.com. DOI: 10.1002/jmri.28826

Received Dec 13, 2022, Accepted for publication May 12, 2023.

*Address reprint requests to: O.B., INSA LYON Bâtiment Léonard de Vinci, 21 Avenue Jean Capelle, 69621 Villeurbanne Cedex, France.
E-mail: olivier.beuf@creatis.univ-lyon1.fr

From the [1]Univ Lyon, INSA-Lyon, Université Claude Bernard Lyon 1, CNRS, Inserm, CREATIS UMR 5220, U1294, Lyon, France; [2]Department of Anatomopathology, CHU Edouard Herriot, Hospices Civils de Lyon, Lyon, France; and [3]Department of Hepatology, CHU Edouard Herriot, Hospices Civils de Lyon, Lyon, France

Additional supporting information may be found in the online version of this article

guides the treatment strategy.[1] Overall, estimated 1.5 billion people worldwide have CLD, and 2 million people die from cirrhosis and liver cancer per year.[2,3] Although liver biopsy carries an approximate 2% mortality with a high risk of major bleeding, followed histological analysis is still the reference method for the diagnosis of CLD, but its invasiveness limits its clinical use.[4] Therefore, an alternative noninvasive, sensitive and specific method for population screening and monitoring remains an unmet medical need.

Diffusion-weighted imaging (DWI) derived from MRI has been increasingly used in liver examinations because of the excellent insight offered by the quantitative measurement of water molecule movement in different microenvironments.[5] The respective water diffusion is intrinsically linked to the degree of liver fibrosis.[5] Such methods have been investigated extensively in the literature.[5–12] Specifically, CLD patients have lower apparent diffusion coefficient (ADC) values than healthy individuals since the abnormal liver parenchyma increase the liquid impedance.[13] However, the diagnostic value of ADC in the evaluation of fibrosis remains relatively controversial.[14,15] Annet et al demonstrated that the lower ADC values in fibrotic livers were caused mostly by perfusion alterations rather than decreased extra-vascular diffusion.[14] Meanwhile, Yoshimaru et al showed ADC-values were undervalued in cirrhotic tissue and tumors due to the restriction of molecular movement in a high cellularity structure.[15] In consequence, the simple ADC model shows difficulty in describing such multifactorial synergy mechanisms. Hence, in recent diffusion MRI studies, several advanced diffusion models were proposed to solve this problem, such as intravoxel incoherent motion (IVIM),[16] stretched exponential model (SEM),[17] statistical diffusion model (Stat_D).[18]

In 1988, Le Bihan et al proposed the IVIM model, which quantified diffusivity separated into diffusion (D), pseudo-perfusion (D^*) effects, and perfusion fraction (f).[16] Leporq et al demonstrated that D and D^* significantly decreased between early and advanced fibrosis groups.[5] Lefebvre et al also reported that f was strongly correlated with inflammation and fibrosis after accounting for fibrosis and steatosis.[6] However, an incomplete understanding of the IVIM mechanism in the tissue structure led to difficulties in separating the pseudo-perfusion and diffusion effects.[7]

In 2003, Bennett et al introduced SEM in the brain that expanded the bi-exponential compartments to multi-compartments with fewer parameters than IVIM.[17] The SEM model evaluated the average diffusion rate through distributed diffusion coefficient (DDC) and diffusion heterogeneity (α).[17] Park et al reported that DDC in SEM presented a higher diagnostic function for hepatic fat staging compared with parameters in IVIM and ADC.[8] Moreover, SEM may be regarded a promising method for fibrosis staging requiring fewer b-values than IVIM, but the physical relevance of α remains unclear.[9]

In 2003, Yablonskiy et al proposed a phenomenological Stat_D that describes the ADC (D_s) and its distribution (σ).[17] Zhou et al explored the application of non-Gaussian models for the prognosis of colorectal cancer.[12] Significantly lower values of σ were observed in the response group before treatment.[12] Although this model has not yet been applied to study the liver, the model's effectiveness is still in doubt because one parameter is hard to estimate while capturing both perfusion and the non-Gaussian phenomenon.

In this context, the aim of the present study was to investigate the effects of different fitting methods on the measurement of diffusion parameters from IVIM, SEM, and Stat_D models[16–18] and to study their relationship with diffuse parenchyma liver disease-related features, particularly for fibrosis assessment.

Materials and Methods

Numerical Simulation

To evaluate numerically the accuracy of fitted parameters with different noise level conditions according to the diffusion model function and the different fitting methods, we simulated diffusion MRI signals with multiple b-values for all the aforementioned diffusion models. All simulations were implemented in MATLAB R2019b (The MathWorks Inc., Natick, MA, USA). For each voxel, the diffusion parameters can be represented as $S_i = S_0 \times \mathrm{L}(\mathbf{c})$, where S_i represents the signal intensity at a given b_i-value, S_0 represents the signal intensity without a diffusion gradient, and c and L(**c**) are the model parameters and model function, respectively. First, the Gaussian distribution randomly generated the coefficient with a certain mean and standard deviation, as shown in Table 1. Then, the advanced diffusion model signals were calculated with their function, as described in Table 2.

The noise levels were impacted differently according to the different b-values. We thus considered adding various inherent noises that we characterized through the Rician–STD method[19] from 85 patients DWI detailed in MRI acquisition.[20] The simulated diffusion signals were then corrupted by Rician noise, which was closer to the actual noise power than the Gaussian distribution since magnitude MRI data were used. The probability distribution for the noisy signal can be calculated as follows:

$$NS_i = \sqrt{S_i + \sigma R_i \times \mathrm{randn(n)}^2 + \sigma I_i \times \mathrm{randn(n)}^2}, i = 1, \ldots, 12, \quad (1)$$

where NS and S represent the noisy signal and pure, noiseless signal, respectively, i is the index of b-values, and σR_i and σI_i are averaged standard deviation at specific b-values for the real and imaginary parts, respectively. In practice, the real and imaginary parts shared the same values simplifying the noise model. After generating the ground truth and noisy signal, the parameters were estimated using NLS, segmented NLS, and Bayesian fitting methods. The performance of the three estimation methods was validated by mean squared error on fitted parameters and mean absolute percentage error on signal.

TABLE 1. Major parameter settings in the simulation

	Model	Parameters	Values
b-values set (s/mm^2)	-	-	0, 10, 20, 40, 60, 80, 100, 200, 300, 400, 600, 800
	STD	D_s($\times 10^{-3}$ mm^2/s)	1.34 ± 0.81
		σ($\times 10^{-3}$ mm^2/s)	0.37 ± 0.18
	SEM	DDC($\times 10^{-3}$ mm^2/s)	1.353 ± 0.268
		α	0.569 ± 0.073
	IVIM	f(%)	24.6 ± 7.28
		D($\times 10^{-3}$ mm^2/s)	0.91 ± 0.19
		D*($\times 10^{-3}$ mm^2/s)	76.2 ± 7.98

Stat_D = statistical diffusion model; SEM = stretched exponential model; IVIM = intravoxel incoherent motion. In the simulation, the same b-values were used as in the in vivo study. The parameters were assumed to follow Gaussian distribution. The data are represented as median ± standard deviation.

TABLE 2. Diffusion-based MRI model parameters and their structural proxy

Diffusion MRI Model	Parameters	Definition (Structural Proxy)	Function
Stat_D	D_s (mm^2/s)	Position of distribution maxima ADC (limited isotropic diffusion)	$\frac{S_i}{S_0} = \exp\left(-\mathbf{b} \times D_s + \frac{1}{2} \times \mathbf{b}^2\sigma^2\right)$
	σ (mm^2/s)	Distribution width of ADC (non-Gaussian diffusion)	
SEM	DDC (mm^2/s)	Distributed diffusion coefficient (limited isotropic diffusion)	$\frac{S_i}{S_0} = \exp[-(\mathbf{b} \times \mathrm{DDC})^{\alpha}]$
	α	Diffusion (heterogeneity perfusion)	
IVIM	f	Vascular volume fraction (isotropic diffusion fraction)	$\frac{S_i}{S_0} = (1-f)\exp(-\mathbf{b} \times D) + f \times \exp\left(-\mathbf{b} \times D^*\right)$
	D (mm^2/s)	Pure diffusion (limited isotropic diffusion)	
	D* (mm^2/s)	Perfusion-related diffusion (perfusion)	

Stat_D = statistical diffusion model; SEM = stretched exponential model; IVIM = intravoxel incoherent motion.

Patient Population

In this study, the patients were retrospectively enrolled from a database of 85 patients with CLD,[20] including alcoholic hepatitis, NASH, and viral hepatitis. This database included conventional diagnostic MRI acquisitions and multiple b-values diffusion acquisition, hepatic blood biomarkers, fibroscan results, and histology. This database was built in our institution.[20] Our institutional review board approved this retrospective study and the requirement to obtain informed consent was waived. Information on the patient population is summarized in Table 3. Inclusion criteria were age superior to 18 years; CLD based on clinical history or prior examination; need for liver biopsy and liver MRI imaging. Exclusion criteria included liver transplantation within the last 6 months, acute liver disease, pregnancy and patient with claustrophobia, metallic implant, pacemaker or coagulation disorders.

Diffusion-Weighted MRI Acquisition

All patients underwent an MRI examination with a 3-Tesla system (GE MR750, GE Healthcare, Chicago, IL, USA). The DWI sequence was a spin echo-echo planar imaging (SE-EPI) enhanced

TABLE 3. Patient characteristics

		Values
General information	Gender	Male: N = 49 Female: N = 36
	Age (years)	47.9 ± 15.5 (20–80)
	Height (m)	1.70 ± 0.11
	Weight (kg)	76.8 ± 17.99
Laboratory parameters	ASAT(U/L)	51.25 ± 39.28
	ALAT(U/L)	83.80 ± 89.48
	ISHAK score	F0: 9, F1: 20, F2: 15 F3: 15, F4: 16, F5: 8, F6: 2
	Inflammation	A0: 28 A1: 47, A2: 10
Clinical etiology	Alcohol	23
	NASH	23
	Viral hepatitis	B: 24 C: 21 Others: 4
	Liver transplant	7

ASAT = aspartate transaminase; ALAT = alanine transaminase; NASH = nonalcoholic fatty liver disease. Data are represented as median ± standard deviation, with the unit in parentheses and range in brackets.

TABLE 4. MRI acquisition parameters

Parameters	Sequence
	SE-EPI-eDWI
b-values (s/mm^2)	0, 10, 20, 40, 60, 80, 100, 200, 300, 400, 600, 800
TE (msec)	54.3
TR (msec)	2050
Acquisition matrix size	128 × 96
Matrix size	256 × 256
FOV (mm^2)	400 × 300
Signal average	2, 2, 2, 2, 3, 3, 4, 5, 6, 7, 8, 9
Slice thickness (mm)	8
Acquisition time (s)	312

SE-EPI-eDWI = spin echo-echo planar imaging-enhanced diffusion-weighted imaging; TE = echo time; TR = repetition time; FOV = field of view. Adjacent slices were joined with no gap between the slices.

DWI (eDWI) acquired in the transverse plane using a tetrahedral gradient encoding (i.e., four combinations of x, y, and z gradients within 50 mT/m^{-1}).[21] The acquisition parameters of the diffusion MRI protocols are listed in Table 4. The MRI signal was acquired with 128 × 96 matrix, a field of view (FOV) of 400 × 300 mm^2, and joined slices had a slice thickness of 8 mm and were reconstructed in 256 × 256 by zero filling to a FOV of 400 × 400 mm^2. No motion correction or fat saturation pulses were applied.

Diffusion Parameter Fitting Methods

Under the additional magnetic field gradients, diffusion signal attenuation is caused by the phase dispersion of transverse magnetization.[5] This diffusion decay can be decomposed into three compartments: perfusion (eg D^*, α, σ), limited isotropic diffusion (eg D, D_s, DDC), and non-Gaussian diffusion (eg σ), depending on the water proton surroundings (microcirculation, tissue fluid, and intra- or extracellular membranes) (Supplementary Material). The contribution of the parameters of each model in the triangular behaviors is listed in Table 2. The MRI diffusion-weighted signals were acquired for the pre-defined *b*-values indexed with $i = 1, 2, 3, \ldots, 12$. The parameters (Table 2) were fitted using a nonlinear least squares (NLS) method, a combination of an NLS fit with a segmented approach as a first step to initiate NLS guess values (segmented NLS), and Bayesian methods.[22,23] The following equation describes the process for the IVIM model (Table 2). In this case, the model function is given by equation:

$$\frac{S_i}{S_0} = (1-f) \times \exp(-b \times D) + f \times \exp\left(-b \times D^*\right), \quad (2)$$

where S_i represents the signal intensity at a given *b*-value and S_0 represents the signal intensity when no pulsed diffusion gradient is applied.

NLS METHOD. The NLS method iteratively finds the best fit for the given nonlinear data by minimizing an objective function, such as in Equation (3) constituted by the residual sum of squares, i.e., the sum of the squares of residuals (deviation of estimated model from actual acquired data):

$$\sum_{i \in b \text{ values set}} \left(S_i - \widehat{S}_i\right)^2, \quad (3)$$

where $\widehat{S}_i$ is the reconstructed signal with the estimated parameters in each iteration. The parameters are updated by the gradient descent until convergence or until reaching the maximum number of allowed iterations.

SEGMENTED NLS METHOD. For the NLS methods to work properly, the parameters need to be weakly correlated.[22] However, in the diffusion models studied, most of the model parameters are highly correlated, which leads to an often ill-posed problem and results in a high noise level dependence.[23] To help distinguish between the water motion in diffusion from perfusion behavior, the segmented NLS method adopts a piecewise fitting strategy. The D^* is a hundred times higher than D.[23] Thus, the D^* can be negligible when the b-value is high enough ($b \geq b_{th}$). In this case, the signals are considered as nearly pure diffusion. In the first step, the IVIM model is simplified to a mono-exponential model:

$$S_i = S_{b_{th}} \exp\left[(-b + b_{th}) \times \widehat{D}\right] = S_0(1-f)\exp\left(-b \times \widehat{D}\right) = \widehat{A}\exp\left(-b \times \widehat{D}\right)\ (b \geq b_{th}). \quad (4)$$

The perfusion fraction is calculated as $\widehat{f} = 1 - \widehat{A}/S_0$. The parameters are underestimated ($\widehat{D} < D, \widehat{f} < f$). Therefore, the parameter values fitted in this piece can be used as lower bounds for the next steps.

Then, f and D^* were estimated in $b \leq b_{th}$ with fixed D as follows:

$$S_i = S_0\left\{\exp[(1-f)(-b \times D)] + \exp\left[f\left(-b \times D^*\right)\right]\right\}, \left(f > \widehat{f}, b \leq b_{th}\right). \quad (5)$$

BAYESIAN METHOD. The NLS-based methods find the optimized parameters with respect to the residuals. By contrast, the Bayesian approach maximizes the posterior probability with the observed signal, an infinite parametric distribution, and noise distribution.[24] The objective function is defined as:

$$\text{argmax}\, p\left(P, \beta, \Sigma_\beta | S\right) \propto p\left(S \mid P, b, \beta, \Sigma_\beta\right) p\left(P | \beta, \Sigma_\beta\right), \quad (6)$$

where P is a vector of the IVIM's parameters, including, f, D, D^*, S_0, and β, Σ_β, which are the mean values of P and their covariances. In practice, to estimate the full parameters with the Bayesian method in a finite time, a Monte Carlo Markov chain (MCMC) is built, and Metropolis–Hastings sampling with a shrinkage strategy is used to accelerate the MCMC convergence.[25] In Bayesian estimation, the parameters are initialized by the NLS results, and their priors are assumed to be of Gaussian form, except for f, which is supposed to have a uniform distribution.[23]

In Vivo Data Analysis

Based on the MRI acquisition, the different models were used to compute diffusion parameters with the three fitting methods (NLS, segmented NLS and Bayesian) for each voxel within Regions of interest (ROIs). The ROIs were placed in the entire right hepatic lobe to minimize the heartbeat effect in MATLAB R2019b (The MathWorks Inc., Natick, MA, USA). For each patient, five slices were located in the middle of the liver by J.H. with the guidance of B.L. (12 years' experiences) ensuring the largest view of the liver lobe. For post-processing, MR signals were arranged in ascending order into multiple vectors (1 × number of b-values) at each pixel. The mean values in ROI for all parameters were calculated for each patient.

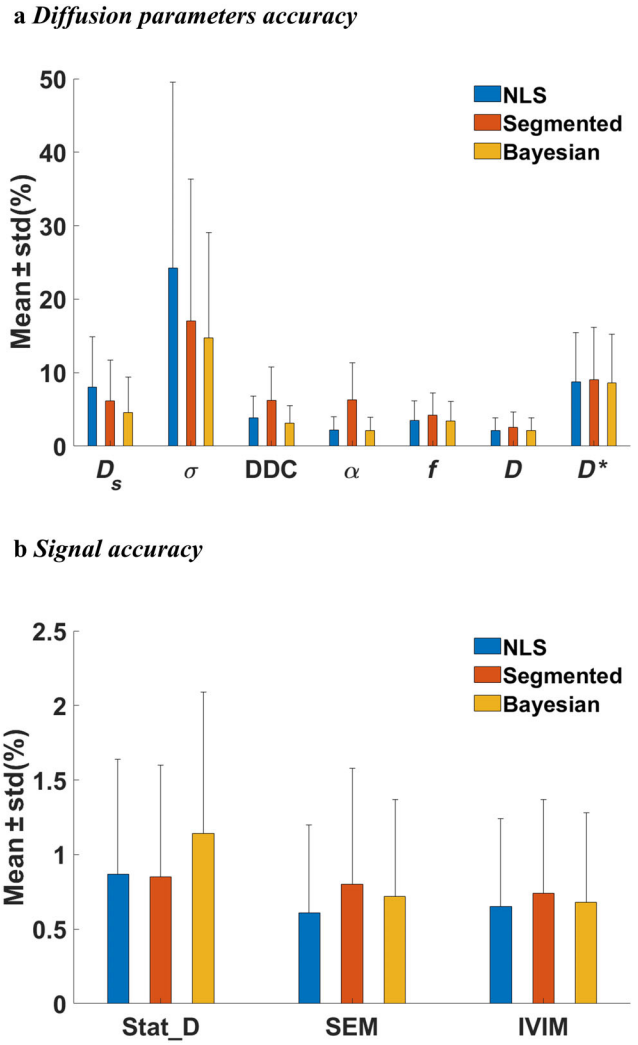

FIGURE 1: Estimation of accuracy in parameters and signal. In the simulation, all parameters fitted by NLS, segmented NLS, and Bayesian methods were compared with the ground truth. (a) Comparison of three estimators for different parameters between ground truth and fitted-parameters based on mean squared error. (b) Comparison of three estimators for signal between ground truth and reconstructed signal based on mean average percentage error. NLS = nonlinear least squares method.

Histology

All patients underwent liver biopsy under ultrasound guidance. A 15G needle was inserted slightly below the bottom right rib cage to obtain the tissue samples. The mean biopsy length was 13.08 ± 2.35 mm (range: 7–18 mm) and the cross-sectional area was 9.14 ± 3.15 mm^2 (range 2.08–18.72 mm^2). Tissue samples were embedded in paraffin after being fixed in buffered formalin. All histological slides were stained with hematoxylin–eosin-saffron, Sirius red, and Perls stain. Histopathological assessment was achieved blinded to any clinical information or MRI result by two

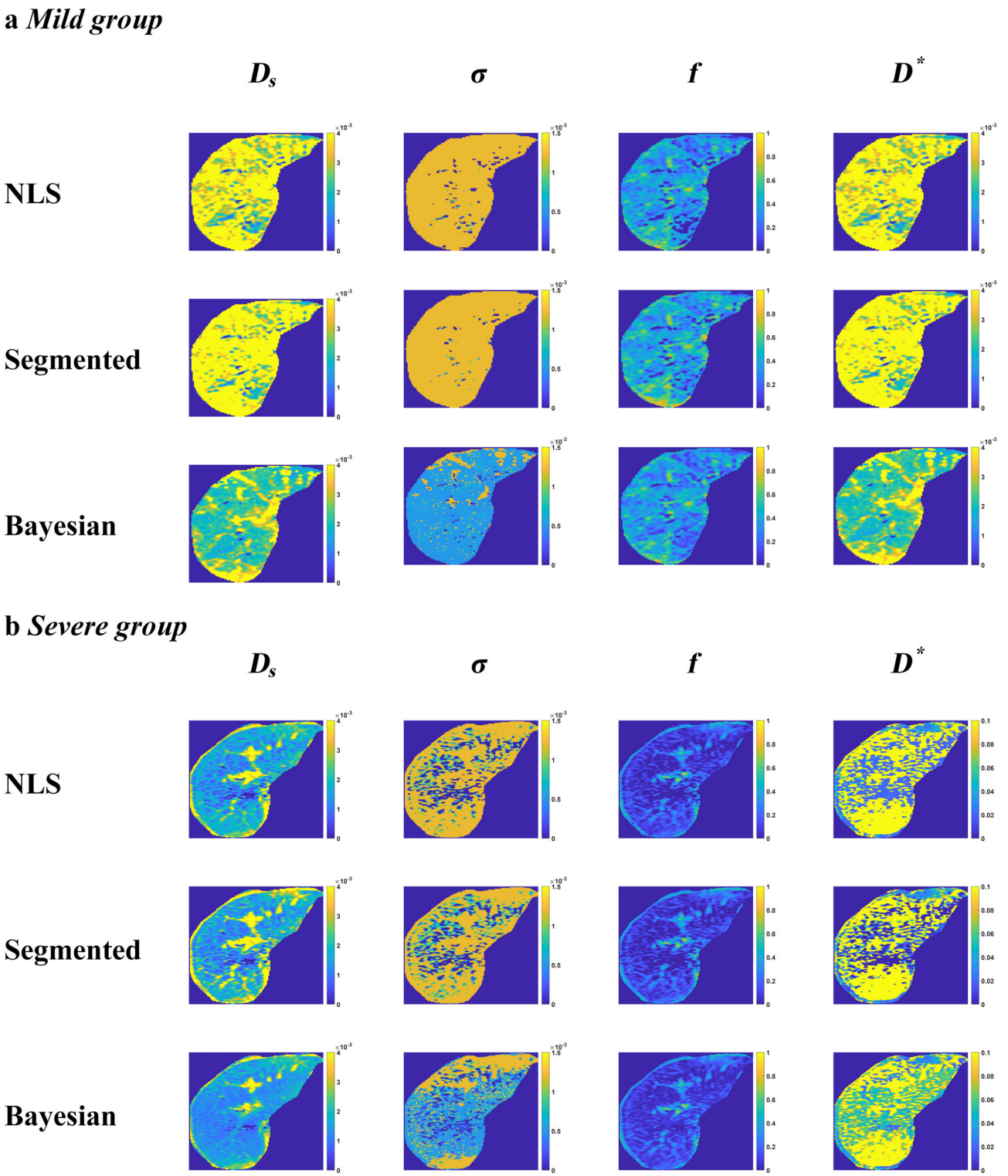

FIGURE 2: Representative diffusion parameters (mm^2/s) fitted by three methods for two fibrosis groups. NLS = nonlinear least squares method.

pathologists (pathologist 1: 20 years of experience and H.V. [co-author]: 10 years of experience) according to Ishak, non-alcoholic fatty liver disease activity score (NAS), and meta-analysis of histological data in viral hepatitis (METAVIR) for fibrosis, steatosis, and inflammation, respectively.[26,27] The histopathologic analysis was reviewed by H.V. and the discrepancies were co-validated. The area of steatosis and fibrosis (in %) were evaluated by H.V. The percentage of steatosis was morphological and semi quantitative (NAS) and the percentage of fibrosis was morphological and quantitative. Image analysis was performed by using a light microscope (Eclipse E400, Nikon France, Champigny, France) equipped with a tri-CDD video camera (Sony, Tokyo, Japan) was determined by morphometric

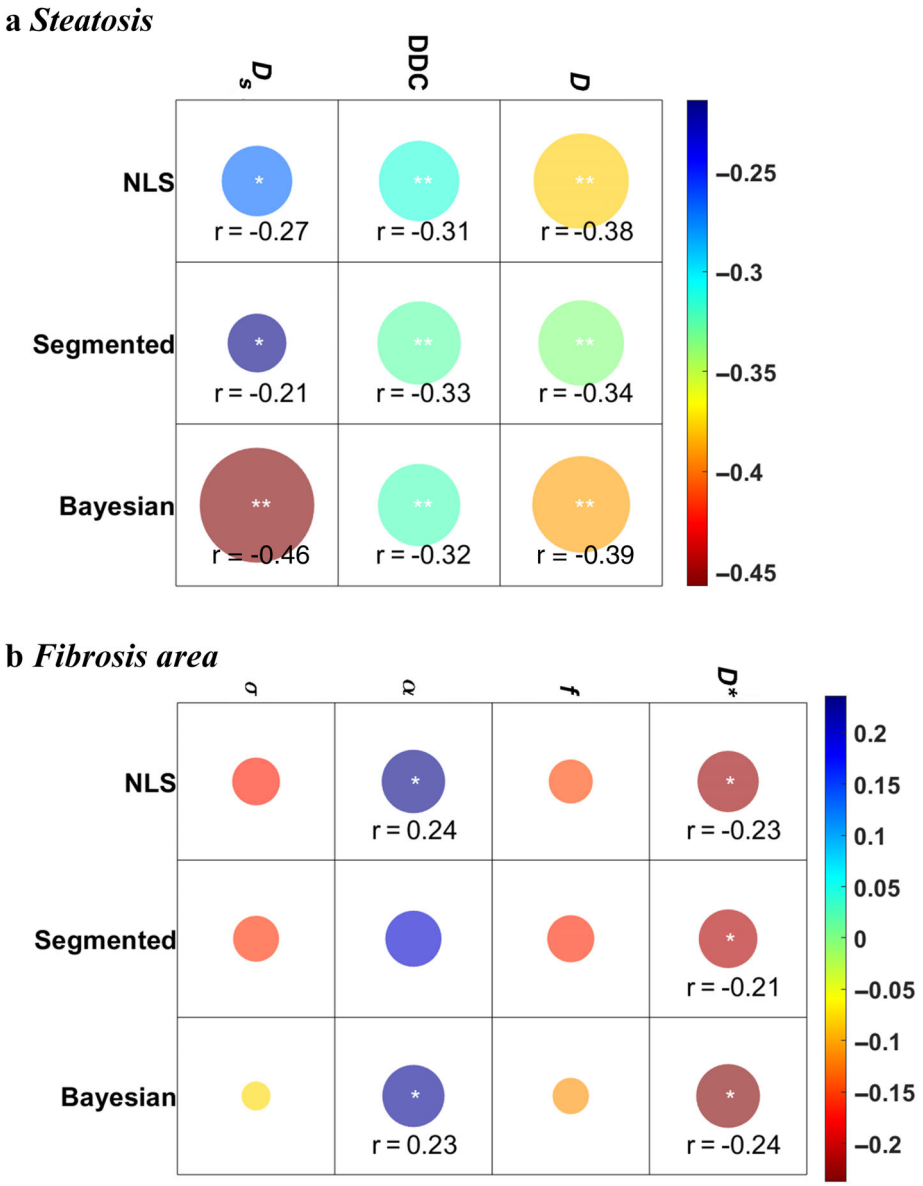

FIGURE 3: Correlation of diffusion parameters with chronic liver disease histology biomarkers for (a) steatosis and (b) fibrosis (the color of the circle reflects the relevance, and the area of the circle reflects the significance; *$P < 0.05$; **$P < 0.01$), when no *r*-value is given, there is no significant correlation. A *P*-value <0.05 was considered statistically significant. NLS = nonlinear least squares method.

analysis (Hisolab, Microvision Instruments, Evry, France). Inflammation was measured by combining the degree of portal necrosis and lobular necrosis based on METAVIR.

Statistical Analysis

Statistical analyses were performed in GraphPad Prism (version 5.0 for Windows, GraphPad Software, San Diego, CA, USA) and MATLAB R2019b (The MathWorks Inc., Natick, MA, USA). To evaluate diffusion parameters in assessing liver fibrosis, we analyzed the results of the three fitting approaches by computing the Spearman correlation coefficients between the diffusion parameter mean values and the fibrosis area. We also evaluated associations between liver steatosis and the diffusion parameters by computing Spearman correlation coefficients between the diffusion parameters and the steatosis area. Based on the Ishak score, the patients were divided into two groups according to fibrosis severity (mild fibrosis [F0–F2] vs. severe fibrosis [F3–F6]) and according to the activity score (no inflammation [A0] vs. hepatitis [A1–A2]). Mann–Whitney *U*-test was used to compare averaged diffusion parameter values for the different groups. A statistical significance level of 0.05 was used, such that any *P*-value below this threshold was deemed significant.

The parameters showing significant differences with $P < 0.01$ between the groups for a given fitting method were combined to build classifiers based on several conventional machine learning methods (Supplementary Material), including linear regression, decision tree (DT), quadratic discriminant (QD), logistic regression, naïve Bayesian (NB), support vector machines (SVMs), and k-nearest neighbor

TABLE 5. Diagnostic values of diffusion parameters in diagnosing mild and severe fibrosis

		NLS	Segmented	Bayesian
$D_s(\times 10^{-3}$ mm^2/s)	Mild	3.11 ± 0.59	3.37 ± 0.58	**2.63 ± 0.60**
	Severe	2.78 ± 0.76	3.03 ± 0.77	**2.18 ± 0.58**
	P	**	**	***
$\sigma(\times 10^{-3}$ mm^2/s)	Mild	1.06 ± 0.11	1.08 ± 0.10	**0.85 ± 0.20**
	Severe	1.00 ± 0.12	1.01 ± 0.12	**0.71 ± 0.16**
	P	**	**	***
DDC$(\times 10^{-3}$ mm^2/s)	Mild	2.30 ± 0.57	1.37 ± 0.23	2.28 ± 0.56
	Severe	2.04 ± 0.69	1.30 ± 0.25	2.03 ± 0.65
	P	*	0.13	*
α	Mild	0.58 ± 0.07	0.49 ± 0.08	0.58 ± 0.07
	Severe	0.62 ± 0.10	0.54 ± 0.10	0.62 ± 0.09
	P	*	*	0.06
f	Mild	0.22 ± 0.05	0.23 ± 0.05	0.22 ± 0.04
	Severe	0.20 ± 0.06	0.20 ± 0.07	0.20 ± 0.06
	P	*	*	*
$D(\times 10^{-3}$ mm^2/s)	Mild	1.34 ± 0.24	1.30 ± 0.22	1.36 ± 0.23
	Severe	1.24 ± 0.25	1.21 ± 0.23	1.27 ± 0.24
	P	*	0.07	*
$D^*(\times 10^{-1}$ mm^2/s)	Mild	1.18 ± 0.37	0.98 ± 0.33	**1.03 ± 0.34**
	Severe	1.05 ± 0.37	0.89 ± 0.33	**0.84 ± 0.26**
	P	0.11	0.18	**

NLS = nonlinear least squares method. The values are mean values and standard deviation for the average parameters in two groups. A *P*-value <0.05 was considered statistically significant.
*$P < 0.05$;
**$P < 0.01$;
***$P < 0.001$.

(KNN) methods (MATLAB R2019b Classification Leaner; The MathWorks Inc., Natick, MA, USA). The classification task consisted in determining if a patient belongs to a severe or mild fibrosis group using diffusion parameters. The dataset was divided into training (75%) and test subsets (25%) by stratified sampling strategies to guarantee completeness (involving all possibilities) and identities (same proportions as the population). In training, 10-folders cross-validation was used for generalization to avoid the high model bias or overfitting problem. In order to tune the hyperparameters of the aforementioned classification methods, the hyperparameter optimization option was activated in the Hyperparameter Optimization Options toolbox of MATLAB. After training the classifiers, receiver operating characteristic (ROC) analysis with the area under the curve (AUC) was performed on the test subset to evaluate the diagnostic performance in classifying mild or severe fibrosis.

Results

Simulation

The diffusion signals were calculated as the ground truth according to the fixed parameters described in Tables 1 and 2. The average standard deviations of noise given through the Rician–STD method were found to be 6.1, 4.2, 4.2, 4.1, 3.7, 3.6, 3.4, 2.9, 2.6, 2.4, 2.3, 2.5 for *b*-values ranging from 0 to 800 s/mm^2.

The relative errors between the reconstructed signal or fitted parameters and their corresponding ground truth are displayed in Fig. 1 with their mean ± standard deviation plots in order to assess the accuracy performance. The Bayesian fitting method almost systematically improved the

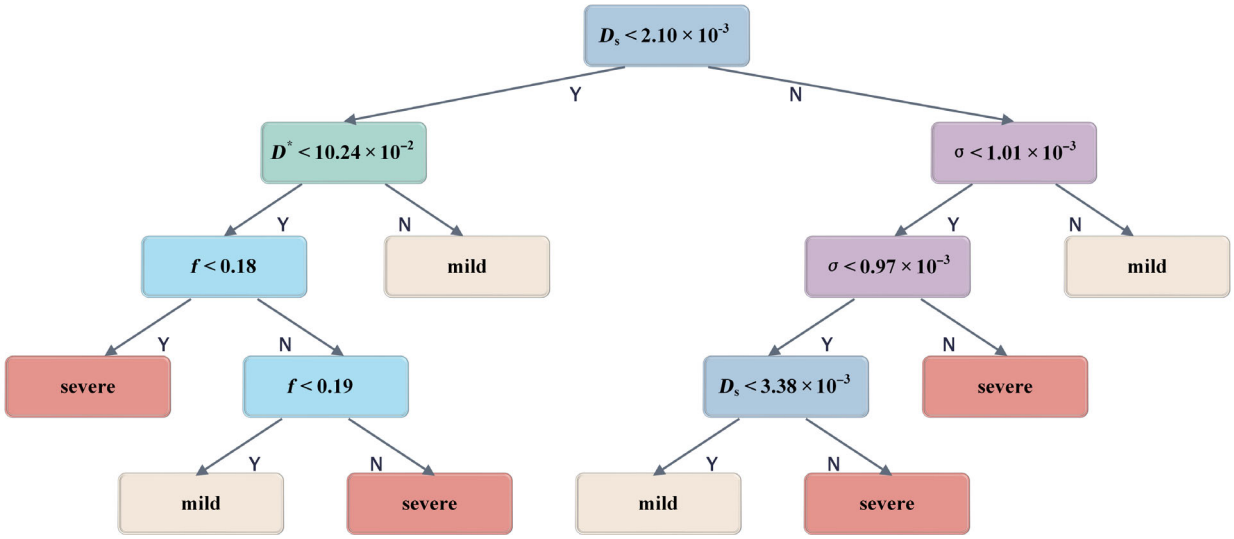

FIGURE 4: Decision tree structure. The unit of parameters (D_s, σ, and D^*) are mm^2/s.

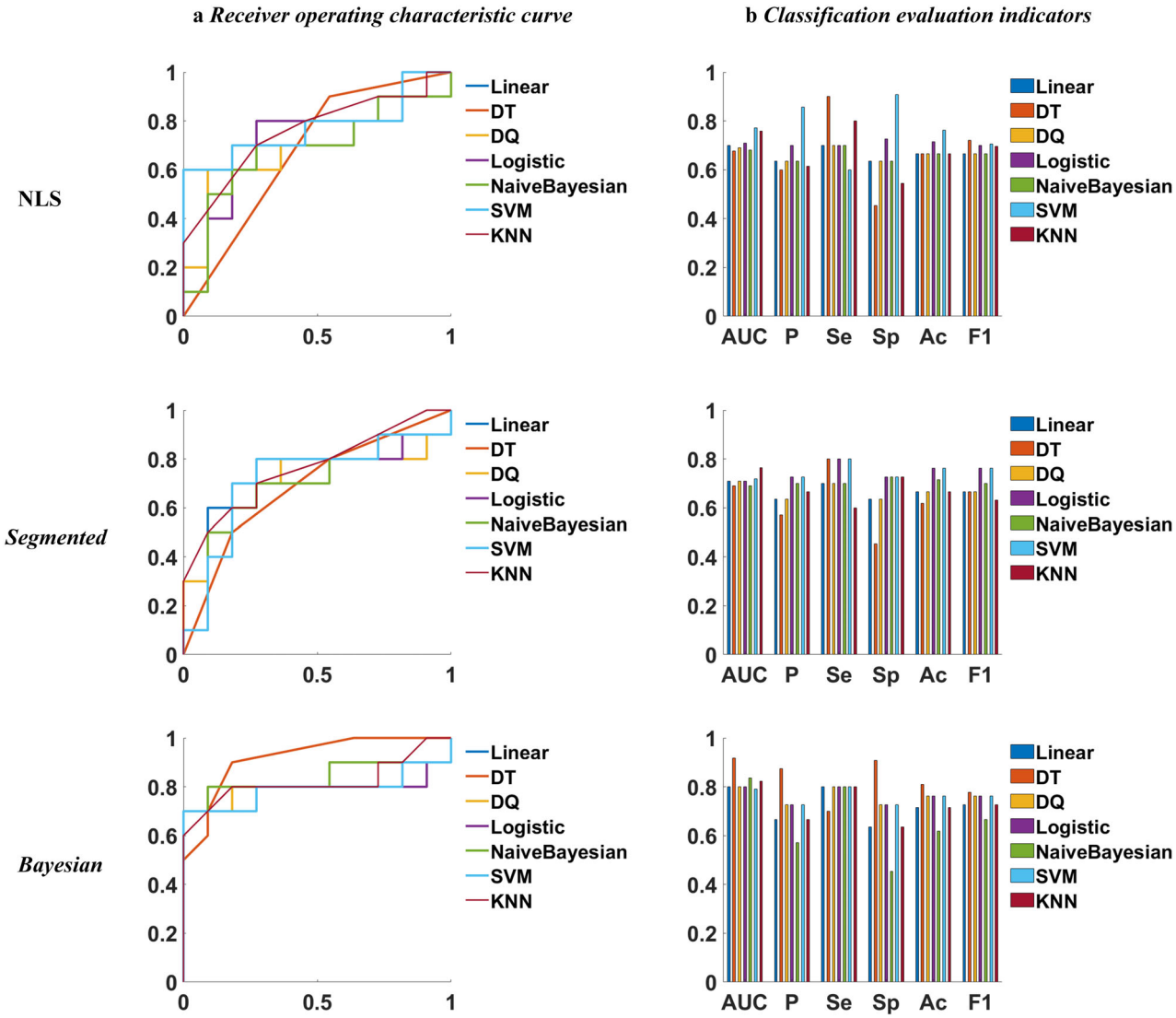

FIGURE 5: Diagnostic values of diffusion parameters in the classification of mild and severe fibrosis. NLS = nonlinear least squares method; DT = decision tree; QD = quadratic discriminant; SVM = support vector machine; KNN = K-nearest neighbor; AUC = area under the curve; P = precision; Se = sensitivity; Sp = specificity; Ac = accuracy; F1 = F1 score.

accuracy of the parameters compared with the NLS-based method (Fig. 1a,b). The relative errors in pure diffusion parameters were less than 10%, and in signal amplitudes even less than 2%. However, there were greater errors with advanced diffusion parameters, especially for σ and D^*.

In Vivo Study

Figure 2 shows the representative diffusion parameters fitted by the three methods for patients with severe and mild fibrosis. Figure 3 summarizes the statistically significant correlation coefficients that were found between limited isotropic diffusion parameters and steatosis (Fig. 3a) or fibrosis area (Fig. 3b). A higher correlation was observed for parameters fitted by the Bayesian method compared with the other methods. The highest correlation was found with the Bayesian method for D_s in the Stat_D model that showed the strongest and statistically significant negative correlation with steatosis ($r = -0.46$). For fibrosis area, a weak but still significant correlation (α: $r = 0.23$, D^*: $r = 0.24$) was found with the parameters fitted with the Bayesian method.

Significant differences were found between the groups with different degrees of fibrosis: D_s, D_{app} as well as σ, α, and D^*(Table 5). In addition, statistically significant differences were only found for diffusion parameter estimations obtained with the Bayesian inference method (D_s and σ). When considering inflammation groups, no significant differences between groups were found for the different fitted parameters (no inflammation [A0] vs. hepatitis [A1–A2], P-values ranged from 0.11 to 0.95). Decision tree with Bayesian fitted parameters, as shown in Fig. 4, achieved the best AUC. The AUC was 0.92 (sensitivity = 0.91 and specificity = 0.70), as shown in the ROC curve in Fig. 5.

Discussion

In this work, we evaluated the effect of different fitting methods on the quantification of diffusion parameters from different models. Compared with the NLS-based method, the Bayesian approach provided greater accuracy in diffusion parameter estimation and fibrosis classification.

The present numerical experiments conducted on simulated signals demonstrated that the Bayesian approach performed better than the NLS-based methods for most parameter estimations. Bouhrara et al also reported similar results for the IVIM and SEM models in a simulation study.[28] The Bayesian method systematically outperformed the NLS-based method in parameter estimation, probably because the Bayesian method reduced the influence of noise on parameters according to the prior and also because it started from the NLS-based estimations.[28] The Bayesian approach may constrain the signal deviations in a larger solution space than the NLS method. To reduce the residual, the NLS solver moves along the gradient descent direction. The algorithm tends to optimize the parameters that contributed the most to the model residual reduction and may remain at a saddle point since the parameter change is not always linearly continuous with signal residuals. With a combination of parameter distribution and knowledge regularization, Bayesian regression self-adaptively updated the parameters. Despite the lower error obtained by the Bayesian method, advanced parameters like σ and D^* are observed with greater errors for all estimators. This result is consistent with the finding given in the literature that the D^* is sometimes associated with inflammation activity.[29] Sensitivity of the parameter estimation to noise and the use of b-values resulted in inaccurate parameter estimation.

Concerning the segmented method, which shared the same optimization algorithm as the NLS, the approximation made for the signals at each step could inevitably introduce systematic errors. In low-noise conditions, the segmented methods have lower accuracy than NLS in terms of signal or parameters. When additional noise becomes important, the segmented NLS method improved the accuracy of the statistical diffusion model. This may partly demonstrate that the segmented NLS method may help obtain quality and correct estimations using the particular b-values at each step. In other words, the segmented NLS method improved the performance in comparison with the NLS method when parameters were difficult to estimate (i.e., are correlated) and in the presence of noise.

Since fibrosis can be accompanied by fat accumulation in CLD, we performed a correlation study to evaluate the confounding effect of fat on diffusion parameters in the assessment of fibrosis. As already found by other studies,[12,30] we found a strong correlation between parameters related to isotropic limited diffusion and steatosis. This effect can be explained by the additional restriction of proton motion due to the fat vesicles. Indeed, all "pure" diffusion parameters fitted by the three methods decreased gradually with steatosis severity.

There was a significant correlation between perfusion-related diffusion parameters and fibrosis. In this in vivo study, diffusion parameters estimated with the Bayesian method could lead to differences between groups of patients with varying degrees of liver fibrosis. Statistically significant differences were observed for D_s, σ, D^*, and f values between patients with mild vs. severe fibrosis using the Bayesian method. We also found that D_s values were significantly lower in the severe fibrosis group than in the mild fibrosis group. This finding may support the notion that both fibrosis and steatosis decrease the limited isotropic diffusion parameters, and fibrosis may impact the limited isotropic diffusion, non-Gaussian diffusion, and perfusion parameters in independent ways.

Several previous studies have focused on staging the grade of fibrosis associated with inflammation and steatosis.[12,28–31] The grading of fibrosis is difficult to guarantee when using only the ADC parameters.[32] In the present study, D_s, σ, D^*,

and f were used to train the variety of classifiers. For the classification between mild and severe fibrosis, the AUC of multiple classifiers used parameters computed with the Bayesian approach, has comparable values to the NLS-based method. In particular, the decision tree classifier achieved the best diagnostic performance with parameters fitted by the Bayesian method. This result may indicate that the accuracy of the fibrosis classification was also influenced by the estimation method. The parameters of each model tested individually were evaluated for their ability to classify fibrosis grade, but none of them provided better results than the combination of parameters from different models in our data. In this regard, many studies have shown that some diffusion parameters can be used to stage liver fibrosis, but they were all conducted on the statistical level (as the first study on in vivo data of this contribution) and did not perform a classification task.[31–34] The decision tree could allow us to get a clearer picture of the relevance of the different fitted parameters. Based on decision tree, D_s could be routinely monitored as a non-invasive screening reference for fibrosis. On the successfully found classifier, D_s have two nodes in 4 depth decision tree and appear at the head of the decision tree. The nodes closer to the root are more representative and understandable as well as the purity of the nodes are also related to the importance of features. For descendant nodes, the decision tree is not straightforwardly readable, given that it used a combination of different parameter level to refine the decision. For example, f values were used for classification on both layer 3 and layer 4. However, we have not found a significant correlation between fibrosis severity and σ values. This later result may support that some advanced parameters are non-linearly correlated with fibrosis severity. Despite the very good classification results achieved by the decision tree, four patients from the test set were not well-classified. In our data, the etiologies of CLD among patients were numerous and we suspect that for these patients impaired vascularization (for one misclassified patients), high level of steatosis (for two misclassified patient), or focal lesion (for one misclassified patient) may have had an impact on diffusion impedance, which was challenging for the classification.

Limitations

We did not consider the imaging gradient effect on low b-values in the simulation study. Indeed, this could be an additive source of signal fluctuation. Second, the cohort of patients was small including different etiologies of CLDs (such as nonalcoholic steatohepatitis [NASH], viral hepatitis, or alcoholic hepatitis), and it is known that the topography of fibrosis differs according to the etiology (peri-sinusoidal in viral hepatitis vs. centro-lobular in NASH).[35] Consequently, in this work, the etiologies may have introduced some bias in the diffusion parameters for fibrosis evaluation Additionally, due to the limited dataset size, it was not possible to develop individual classifications for fibrosis grades using a complex classifier. Third, this study did not discuss the sampling choice of b-values. Indeed, the present work focused on comparing different estimation approaches and diffusion function models for liver characterization. However, it can be shown that b-value sampling schemes impact the parameter fitting and thus their correlation with liver disease features. In order not to underestimate perfusion-related parameters, low b-values (0–50 s/mm^2) were used in this study as recommended in previous liver studies.[36,37] In the present study, due to insufficient signal-to-noise ratio (SNR), gradient strength value, and liver short T2 value, the MRI scanner was limited in the ability to obtain images at b-values greater than 800 s/mm^2. To keep the acquisition time short and to keep good SNR, DWI data were thus acquired with averages and with the maximum b-value set at 800 s/mm^2. Historically, the model capturing non-Gaussian behavior has been performed with high b-values, even has been reported as 2000 s/mm^2.[31] However, the Stat_D has never been applied to liver fibrosis and therefore the required b-values for this model is not fully established. Finally, spatial resolution may impact IVIM parameter values, particularly f and D^*. Indeed, when voxel size increases, the risk to include large vessels or biliary ducts due to the partial volume effect increases. In this context, another faster-decaying diffusion component may corrupt the bi-exponential model and a third component should be added. To address this issue, different approaches have been proposed. Gambarota et al used a non-negative least squares (NLLS) analysis to determine the number of components in the NLSS spectrum and discarded the first b-values for the fitting step in voxels where three components were present.[7] Another work has suggested to start IVIM modeling at $b = 2$ s/mm^2 instead of 0.[38] Li et al demonstrated that compared with IVIM analysis starting from $b = 2$ s/mm^2, IVIM analysis that included $b = 0$ s/mm^2 led to higher inter-subject variations among healthy young volunteers.[38] In addition, an increased sensitivity of IVIM in detecting liver fibrosis has been demonstrated when starting from $b = 2$ s/mm^2.[38] Another group has suggested to acquire additional sets of very small b-values (typically between 0 and 20 s/mm^2) and performed a tri-exponential analysis.[39] Thus, a future study investigating b-value sampling could be used to enhance the findings of the present work.

Conclusion

In this work, we compared three different fitting methods for the estimation of diffusion parameters in terms of estimation accuracy and relevance for fibrosis evaluation. Based on this analysis, we trained a decision tree combining different advanced diffusion parameters computed with the Bayesian approach to predict severe fibrosis ($F > 2$ based on the ISHAK classification) with an AUC of 0.92. Our results also

demonstrate that the Bayesian approach improves the diagnostic performance of diffusion parameters for assessing liver fibrosis and may confirm the confounding effect of fat in the use of diffusivity (*D*) for assessing liver fibrosis.

Acknowledgments

We warmly thank professor Pierre-Jean Valette (radiologist at "Hospices Civils de Lyon") for his involvement and for facilitating the implementation of this work. This work was supported by the China Scholarship Council (CSC), and LabEx PRIMES (ANR-11-LABX-0063) of Université de Lyon, within the program "Investissements d'Avenir" (ANR-11-IDEX-0007) operated by the French National Research Agency (ANR).

References

1. Roehlen N, Crouchet E, Baumert TF. Liver fibrosis: Mechanistic concepts and therapeutic perspectives. Cell 2020;9:875. https://doi.org/10.3390/cells9040875.
2. Cheemerla S, Balakrishnan M. Global epidemiology of chronic liver disease. Clin Liver Dis (Hoboken) 2021;17:365-370.
3. Asrani SK, Devarbhavi H, Eaton J, Kamath PS. Burden of liver diseases in the world. J Hepatol 2019;70:151-171.
4. Thomaides-Brears HB, Alkhouri N, Allende D, et al. Incidence of complications from percutaneous biopsy in chronic liver disease: A systematic review and meta-analysis. Dig Dis Sci 2022;67:3366-3394.
5. Lewis S, Dyvorne H, Cui Y, Taouli B. Diffusion-weighted imaging of the liver: Techniques and applications. Magn Reson Imaging Clin N Am 2014;22:373-395.
6. Annet L, Peeters F, Abarca-Quinones J, Leclercq I, Moulin P, Van Beers BE. Assessment of diffusion-weighted MR imaging in liver fibrosis. JMagn Reson Imaging. 2007;25:122-128.
7. Gambarota G, Hitti E, Leporq B, Saint-Jalmes H, Beuf O. Eliminating the blood-flow confounding effect in intravoxel incoherent motion (IVIM) using the non-negative least square analysis in liver. Magn Reson Med 2017;77:310-317.
8. Le Bihan D, Breton E, Lallemand D, Grenier P, Cabanis E, Laval-Jeantet M. MR imaging of intravoxel incoherent motions: Application to diffusion and perfusion in neurologic disorders. Radiology 1986;161:401-407.
9. Bennett KM, Schmainda KM, Bennett R, Rowe DB, Lu H, Hyde JS. Characterization of continuously distributed cortical water diffusion rates with a stretched-exponential model. Magn Reson Med 2003;50:727-734.
10. Yablonskiy DA, Bretthorst GL, Ackerman JJH. Statistical model for diffusion attenuated MR signal. Magn Reson Med 2003;50:664-669.
11. Leporq B, Saint-Jalmes H, Rabrait C, et al. Optimization of intra-voxel incoherent motion imaging at 3.0 tesla for fast liver examination. J Magn Reson Imaging 2015;41:1209-1217.
12. Lefebvre T, Hébert M, Bilodeau L, et al. Intravoxel incoherent motion diffusion-weighted MRI for the characterization of inflammation in chronic liver disease. Eur Radiol 2021;31:1347-1358.
13. Le Bihan D. What can we see with IVIM MRI? Neuroimage 2019;187:56-67.
14. Park JH, Seo N, Chung YE, et al. Noninvasive evaluation of liver fibrosis: Comparison of the stretched exponential diffusion-weighted model to other diffusion-weighted MRI models and transient elastography. Eur Radiol 2021;31:4813-4823.
15. Seo N, Chung YE, Park YN, Kim E, Hwang J, Kim MJ. Liver fibrosis: Stretched exponential model outperforms mono-exponential and bi-exponential models of diffusion-weighted MRI. Eur Radiol 2018;28:2812-2822.
16. Fujimoto K, Noda Y, Kawai N, et al. Comparison of mono-exponential, bi-exponential, and stretched exponential diffusion-weighted MR imaging models in differentiating hepatic hemangiomas from liver metastases. Eur J Radiol 2021;141:109806. https://doi.org/10.1016/j.ejrad.2021.109806.
17. Anderson SW, Barry B, Soto J, Ozonoff A, O'Brien M, Jara H. Characterizing non-gaussian, high b-value diffusion in liver fibrosis: Stretched exponential and diffusional kurtosis modeling. J Magn Reson Imaging 2014;39:827-834.
18. Zhou Y, Zhang HX, Zhang XS, et al. Non-mono-exponential diffusion models for assessing early response of liver metastases to chemotherapy in colorectal cancer. Cancer Imaging 2019;19:1-11.
19. Coupé P, Manjón JV, Gedamu E, Arnold D, Robles M, Collins DL. Robust Rician noise estimation for MR images. Med Image Anal 2010;14:483-493.
20. Liu J, Gambarota G, Shu H, et al. On the identification of the blood vessel confounding effect in intravoxel incoherent motion (IVIM) diffusion-weighted (DW)-MRI in liver: An efficient sparsity based algorithm. Med Image Anal 2020;61:101637. https://doi.org/10.1016/j.media.2020.101637.
21. Finkelstein A, Cao X, Liao C, Schifitto G, Zhong J. Diffusion encoding methods in MRI: Perspectives and challenges. Investig Magn Reson Imaging 2022;26:208-219.
22. Sigmund EE, Cho GY, Kim S, et al. Intravoxel incoherent motion imaging of tumor microenvironment in locally advanced breast cancer. Magn Reson Med 2011;65:1437-1447.
23. Jalnefjord O, Andersson M, Montelius M, et al. Comparison of methods for estimation of the intravoxel incoherent motion (IVIM) diffusion coefficient (D) and perfusion fraction (f). Magn Reson Mater Phys Biol Med 2018;31:715-723.
24. Gustafsson O, Montelius M, Starck G, Ljungberg M. Impact of prior distributions and central tendency measures on Bayesian intravoxel incoherent motion model fitting. Magn Reson Med 2018;79:1674-1683.
25. Rodrigues SG, Montani M, Guixé-Muntet S, De Gottardi A, Berzigotti A, Bosch J. Patients with signs of advanced liver disease and clinically significant portal hypertension do not necessarily have cirrhosis. Clin Gastroenterol Hepatol 2019;17:2101-2109.
26. Arjmand A, Tsipouras MG, Tzallas AT, Forlano R, Manousou P, Giannakeas N. Quantification of liver fibrosis—A comparative study. Appl Sci 2020;10:447. https://doi.org/10.3390/app10020447.
27. Yin Z, Murphy MC, Li J, et al. Prediction of nonalcoholic fatty liver disease (NAFLD) activity score (NAS) with multiparametric hepatic magnetic resonance imaging and elastography. Eur Radiol 2019;29:5823-5831.
28. Bouhrara M, Reiter DA, Spencer RG. Bayesian analysis of transverse signal decay with application to human brain. Magn Reson Med 2015;74:785-802.
29. Leitão HS, Doblas S, d'Assignies G, et al. Fat deposition decreases diffusion parameters at MRI: A study in phantoms and patients with liver steatosis. Eur Radiol 2013;23:461-467.
30. Besheer T, Razek A, El Bendary M, et al. Does steatosis affect the performance of diffusion-weighted MRI values for fibrosis evaluation in patients with chronic hepatitis C genotype 4? Turk J Gastroenterol 2017;28:283-288.
31. Yang L, Rao S, Wang W, et al. Staging liver fibrosis with DWI: Is there an added value for diffusion kurtosis imaging? Eur Radiol 2018;28:3041-3049.
32. Shin MK, Song JS, Hwang SB, Hwang HP, Kim YJ, Moon WS. Liver fibrosis assessment with diffusion-weighted imaging: Value of liver apparent diffusion coefficient normalization using the spleen as a reference organ. Diagnostics 2019;9:107. https://doi.org/10.3390/diagnostics9030107.

33. Liang J, Song X, Xiao Z, Chen H, Shi C, Luo L. Using IVIM-MRI and R2* mapping to differentiate early stage liver fibrosis in a rat model of radiation-induced liver fibrosis. Biomed Res Int 2018;2018:4673814. https://doi.org/10.1155/2018/4673814.

34. Kim J, Yoon H, Lee M-J, et al. Clinical utility of mono-exponential model diffusion weighted imaging using two b-values compared to the bi-or stretched exponential model for the diagnosis of biliary atresia in infant liver MRI. PLoS One 2019;14:e0226627. https://doi.org/10.1371/journal.pone.0226627.

35. Graupera I, Thiele M, Ma AT, et al. LiverScreen project: Study protocol for screening for liver fibrosis in the general population in European countries. BMC Public Health 2022;22:1-10.

36. Cohen AD, Schieke MC, Hohenwalter MD, Schmainda KM. The effect of low b-values on the intravoxel incoherent motion derived pseudodiffusion parameter in liver. Magn Reson Med 2015;73: 306-311.

37. Li YT, Cercueil JP, Yuan J, Chen W, Loffroy R, Wáng YX. Liver intravoxel incoherent motion (IVIM) magnetic resonance imaging: A comprehensive review of published data on normal values and applications for fibrosis and tumor evaluation. Quant Imaging Med Surg 2017; 7:59-78.

38. Li T, Che-Nordin N, Wáng YXJ, et al. Intravoxel incoherent motion derived liver perfusion/ diffusion readouts can be reliable biomarker for the detection of viral hepatitis B induced liver fibrosis. Quant Imaging Med Surg 2019;9:371-385.

39. Chevallier O, Zhou N, Cercueil J, He J, Loffroy R, Wáng YXJ. Comparison of tri-exponential decay versus bi-exponential decay and full fitting versus segmented fitting for modeling liver intravoxel incoherent motion diffusion MRI. NMR Biomed 2019;32:e4155. https://doi.org/10.1002/nbm.4155.